CFA/VISHNO 2016

Streaming non linéaire : rôle de la composante radiale acoustique

V. Daru[a], D. Baltean Carlès[b], I. Reyt[a] et C. Weisman[b]
[a]DynFluid Lab., ENSAM, LIMSI-CNRS, 151 bd de l'hôpital, 75013 Paris, France
[b]Université Pierre et Marie Curie, LIMSI-CNRS, 4 Place Jussieu, 75252 Paris, France
daru@limsi.fr

The object of this study is the non linear streaming flow created by a mono-frequency standing wave inside a cylindrical resonator. For large values of the nonlinear Reynolds number, the streaming pattern predicted by Rayleigh in the slow regime is distorted and new contra-rotating cells appear in the resonator core. Recently, it has been shown that this behaviour cannot be solely attributed to the effect of inertia.
In the present study it is shown that the radial component of the acoustic velocity plays a key role in the streaming pattern evolution when the flow regime evolves from slow to fast. The acoustic velocity field is computed by solving compressible Navier-Stokes equations under the assumption of isentropic flow. As expected, in the slow regime the radial acoustic velocity varies linearly with the radial space coordinate outside the boundary layer. In the fast streaming regime, this acoustic velocity component is modified greatly and the zone of linear variation is significantly reduced. Moreover the radial acoustic velocity amplitude increases during the fast regime and reaches the same order of magnitude as the radial streaming velocity amplitude. Therefore there exists a strong interaction between acoustic and streaming velocity fields in the fast regime through the radial components which, to our knowledge, was not highlighted until now.

1 Introduction

Acoustic streaming consists of a mean flow, of second order, which is produced by the interaction between the acoustic wave and a solid wall. When the acoustic wave is of small amplitude, slow streaming is produced. In this case, analytical models have been established [1, 2, 3] that show that the streaming velocity has a quadratic dependence in function of the acoustic velocity. When the acoustic velocity amplitude increases, previous experimental and numerical studies [4, 5, 6] have shown that the streaming flow is modified. In certain cases, an additional outer streaming cell is generated. Moreover a change of regime is observed for the streaming velocity dependence upon the acoustic velocity, evolving from a quadratic function in the first (slow) regime to a linear function in the second (fast) regime [7, 8]. In previous studies, the distortion of the streaming pattern when the acoustic amplitude is high was explained as non linear effects of inertia [9, 10], characterised by the non linear Reynolds number $Re_{NL} = (M \times R/\delta_\nu)^2$, where M is the acoustic Mach number, $M = U_{ac}/c_0$, with U_{ac} the maximum acoustic velocity on the axis and c_0 the initial speed of sound, R the radius of the channel and δ_ν the viscous boundary layer thickness. However we showed [7] that the sole effect of inertia cannot be responsible for the observed behaviour.

In the present paper we study the influence of the radial component of the acoustic velocity when streaming flow evolves from the first regime to the second regime. In order to exclude thermal effects, the flow is considered to be isentropic. Two codes are used to this effect. A first code (DNS) is used to solve the full Navier-Stokes compressible equations, providing both the acoustic and streaming fields. The standing wave is excited by imposing a sinusoidal vibration of all resonator walls along the main axis, at frequency corresponding to the lowest resonant acoustic mode of the waveguide. A second code (AMS) solving the time-averaged Navier-Stokes compressible equations was developed, where an acoustic flow field provided by the first code is used as a source term. This code is used to study separately the effect of each source term associated to different correlations of acoustic velocity components. It is shown that the radial component of the acoustic velocity plays a key role in the streaming behaviour when streaming flow evolves from the first regime to the second regime, and that there exists a strong interaction between acoustic and streaming flows in the second regime.

2 Problem description and numerical method

We consider a cylindrical tube of length L and radius R, initially filled with air at pressure p_0 and density ρ_0 equal to 101325 Pa and 1.2 kg/m^3. The viscosity of air is supposed to be constant, $\mu = 1.795\ 10^{-5}\ kgm^{-1}s^{-1}$. In order to initiate an acoustic standing wave in the channel, it is shaken in the longitudinal direction (z), so that a harmonic velocity law is imposed, $\mathbf{V}(t) = (V(t), 0)^T$, with $V(t) = z_p\omega\cos(\omega t)$, ω being the angular frequency and z_p the amplitude of the channel displacement. Acoustic streaming flow is created as a result of the interaction of the imposed plane standing wave and the channel wall. In this paper, streaming flow is calculated from solving a system of averaged equations, over an acoustic period. These equations are derived from the instantaneous system of compressible Navier-Stokes equations, by decomposing each variable into a fluctuating periodic component (i.e. acoustic component) and a steady component (corresponding to the streaming flow), $(\mathbf{v}, \rho, p) = (\overline{\mathbf{v}} + \mathbf{v}', \overline{\rho} + \rho', \overline{p} + p')$, $\mathbf{v}$ being the velocity and the average operator being denoted by an overline:

$$\begin{cases} \dfrac{\partial\overline{\rho}}{\partial t} + \nabla\cdot(\overline{\rho\mathbf{v}}) = -\nabla\cdot(\overline{\rho'\mathbf{v}'}) \\ \dfrac{\partial\overline{\rho\mathbf{v}}}{\partial t} + \nabla\cdot(\overline{\rho\mathbf{v}}\otimes\overline{\mathbf{v}}) + \nabla\overline{p} = \nabla\cdot(\overline{\bar{\bar{\tau}}}) - \nabla\cdot(\overline{\rho'\mathbf{v}'}\otimes\overline{\mathbf{v}} \\ \qquad\qquad + \overline{\mathbf{v}}\otimes\overline{\rho'\mathbf{v}'} + \overline{\rho}\overline{\mathbf{v}'\otimes\mathbf{v}'} + \overline{\rho'\mathbf{v}'\otimes\mathbf{v}'}) \end{cases} \quad (1)$$

where $\bar{\bar{\tau}}$ is the viscous tensor. The averaged products can be obtained by running a previous direct numerical simulation, based on the instantaneous complete system equations [10]. After a periodic state has been attained, at each time step the fluctuating fields can be obtained from the difference between the instantaneous field and the time averaged field, and the time averaged products of these fluctuating quantities can be calculated.

The effect of inertia on nonlinear streaming has been investigated previously [7]. It was shown that the sole effect of inertia cannot be responsible for the acoustic streaming behaviour observed for large values of the nonlinear Reynolds number. In particular, the appearance of other streaming cells, also observed in DNS simulations and experiments do not exist when inertia is the only nonlinear effect taken into account. In the present work, the study is focused on the effect of the acoustic source terms represented by the averaged products in the right hand side of Eq.1. Therefore, streaming flow is calculated as the

steady solution of the linearised version of Eq.1:

$$\begin{cases} \dfrac{\partial \rho_s}{\partial t} + \rho_0 \nabla \cdot (\mathbf{v_s}) = 0 \\ \rho_0 \dfrac{\partial \mathbf{v_s}}{\partial t} + \nabla p_s = \nabla \cdot (\bar{\bar{\tau}}_s) - \rho_0 \nabla \cdot \overline{\mathbf{v}' \otimes \mathbf{v}'} \end{cases} \quad (2)$$

in which third order correlations of fluctuating quantities as well as the compressibility term $\overline{\rho' \mathbf{v}'}$ are also neglected, being one or two orders of magnitude smaller than the second order correlations of fluctuating quantities.

The amplitude value of both components of acoustic velocity are represented over the entire domain $(z, r) \in [0, L] \times [0, R]$ in Figures 1 and 2, at very low streaming flow regime ($z_p = 0.1\ \mu m$). As expected, in the core of the chanel the axial acoustic velocity v'_z has a spatial distribution constant with respect to r (see Figure 3) and sinusoidal with respect to z. The radial acoustic velocity v'_r has a linear variation with respect to r in the core of the chanel (see Figure 4) and its order of magnitude is in the ratio $\pi\delta_\nu/L$ with the axial acoustic velocity v'_z. In the core of the chanel, the associated correlations $\overline{v'_z v'_z}$ and $\overline{v'_r v'_z}$ have a similar behaviour : $\overline{v'_r v'_z}$ is antisymmetric with respect to the $r = 0$ line and has an order of magnitude in the same ratio $\pi\delta_\nu/L$ with the correlation $\overline{v'_z v'_z}$, whose variation is constant in r and sinusoidal in z.

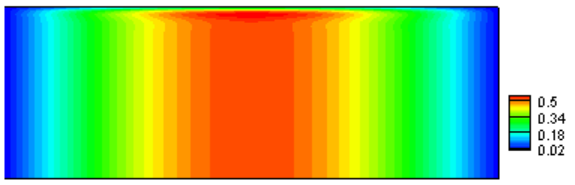

FIGURE 1 – Isolines of the axial acoustic velocity v'_z amplitude colored by its value obtained with the DNS simulation, $z_p = 0.1\ \mu m$.

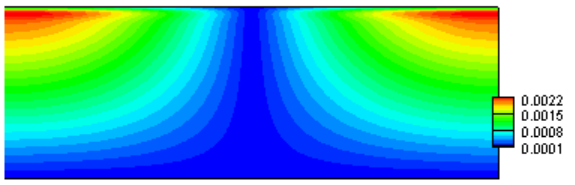

FIGURE 2 – Isolines of the radial acoustic velocity v'_r amplitude colored by its value obtained with the DNS simulation, $z_p = 0.1\ \mu m$.

All results presented below are obtained using a regular mesh of rectangular cells composed of 500 points in the axial direction, and of $5 \times R/\delta_\nu$ points in the radial direction. The time step δt is fixed equal to $8\ 10^{-9}\ s$.

3 Results

Simulations with the DNS code are performed for large tubes ($R/\delta_\nu = 50$, $L = 8.59\ mm$, $R/L = 0.092$) and different forcing amplitudes ($z_p = 0.1, 10$ and $30\ \mu m$), corresponding to configurations ranging from the first streaming regime ($z_p = 0.1\ \mu m$) to the second streaming regime ($z_p = 10$ and $30\ \mu m$). The streaming flow regimes are related to the way

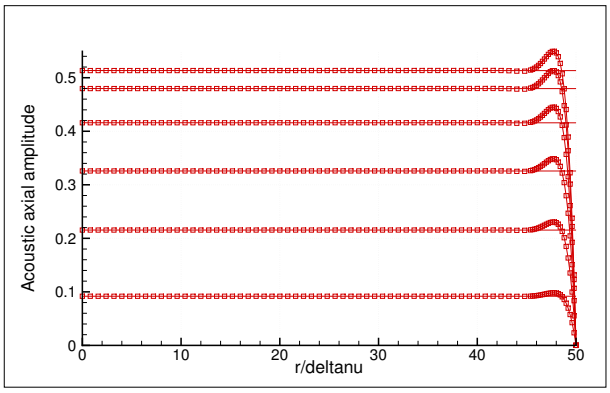

FIGURE 3 – Radial variation of the axial acoustic velocity amplitude at different axial positions, $z_p = 0.1\ \mu m$. Solid lines: linear fit in the core region.

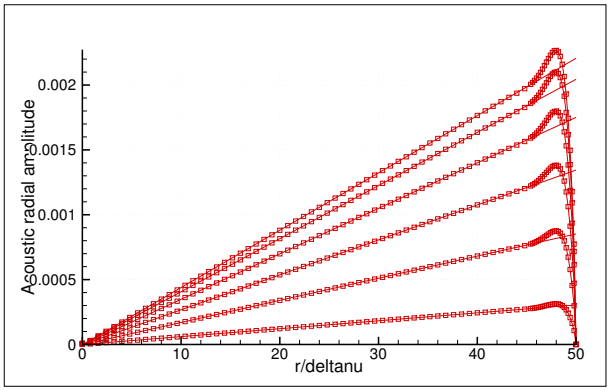

FIGURE 4 – Radial variation of the radial acoustic velocity amplitude at different axial positions, $z_p = 0.1\ \mu m$. Solid lines: linear fit in the core region.

the axial streaming velocity amplitude varies as a function of the axial acoustic velocity amplitude on the axis $r = 0$: in the first regime the variation is parabolic, as in the case of slow streaming, while in the second regime the variation becomes linear [8]. The acoustic Mach numbers vary from $M = 0.001$ to $M = 0.18$.

In the linearised equations system (Eq.2) the source term is the sum of four terms: $\frac{\partial}{\partial z}(\overline{v'_z v'_z})$, $\frac{\partial}{\partial z}\overline{v'_r v'_z}$, $\frac{1}{r}\frac{\partial}{\partial r}(r\overline{v'_r v'_z})$ and $\frac{1}{r}\frac{\partial}{\partial r}(r\overline{v'_r v'_r})$. These terms are taken as source terms associated to the correlations $\overline{v'_z v'_z}$, $\overline{v'_r v'_z}$ and $\overline{v'_r v'_r}$.

In order to analyse the effect of each source term separately, numerical solutions of the linearised equations (Eq.2) are computed considering only one source term at a time.

3.1 Slow streaming flow

We begin by showing simulations performed with a forcing amplitude of $z_p = 0.1\ \mu m$ which corresponds to a slow streaming flow (Regime 1 [8]).

Figure 5 displays isolines of the axial streaming velocity colored by its value and streamlines of the streaming flow obtained when the source term considered is $\frac{\partial}{\partial z}(\overline{v'_z v'_z})$. This source terme is named the axial source term. Figure 6 shows the radial variation of the axial streaming velocity at different axial locations, also obtained with the axial source term. In the core region the variation is parabolic (as confirmed by a polynomial fit), while within the near-wall

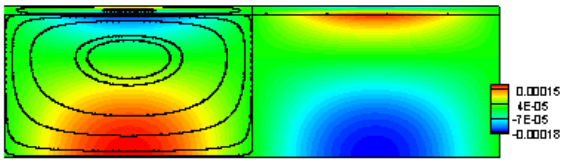

FIGURE 5 – Isolines of the axial streaming velocity colored by its value and streamlines of the streaming flow obtained in the case of the axial source term $\frac{\partial}{\partial z}(\overline{v'_z v'_z})$, $z_p = 0.1\mu m$.

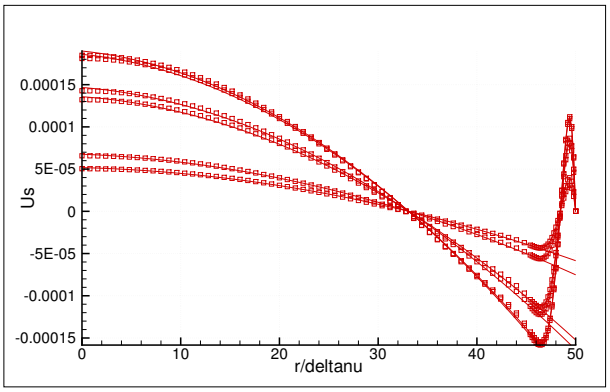

FIGURE 6 – Radial variation of the axial streaming velocity obtained with the axial source term at different axial locations, $z_p = 0.1\mu m$. Solid lines: polynomial fit in the core region.

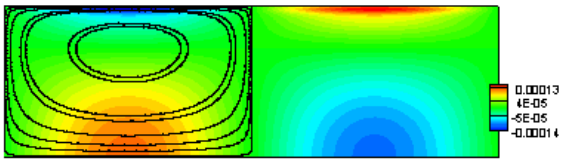

FIGURE 7 – Isolines of the axial streaming velocity colored by its value and streamlines of the streaming flow obtained in the case of the radial source term $\frac{1}{r}\frac{\partial}{\partial r}(r\overline{v'_r v'_z})$, $z_p = 0.1\mu m$.

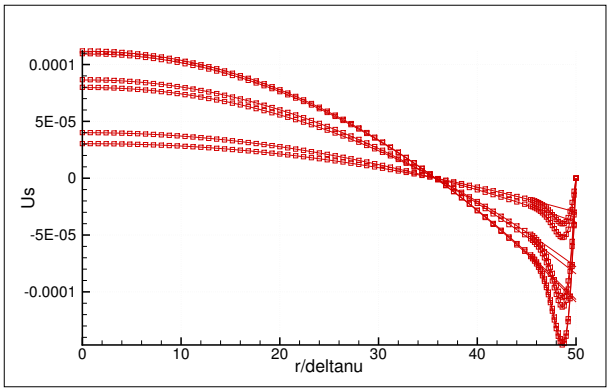

FIGURE 8 – Radial variation of the axial streaming velocity obtained with the radial source term at different axial locations, $z_p = 0.1\mu m$. Solid lines: polynomial fit in the core region.

region the variation changes: the axial streaming velocity increases, changes sign and then decreases and goes to zero on the solid wall (Fig.6). The change of sign in the axial streaming velocity profile corresponds to the presence of a streaming cell in the near-wall region that is called the inner streaming cell. The order of magnitude of the axial streaming velocity maximum value on the $r = 0$ axis and of its minimum value inside the boundary layer are the same. This behaviour can be easily understood by considering the following approximate equation:

$$\mu\frac{1}{r}\frac{\partial}{\partial r}(r\frac{\partial U_{1s}}{\partial r}) = \frac{\partial p_{1s}}{\partial z} + \rho_0\frac{\partial}{\partial z}(\overline{v'_z v'_z}) \quad , \tag{3}$$

whose solution is analytical and describes the axial streaming velocity in cylindrical coordinates, for a large resonator, outside the boundary layer. Both the axial source term and the $\frac{\partial p_{1s}}{\partial z}$ term being independent of the radial coordinate outside the boundary layer, the solution U_{1s} of Eq.3 is parabolic with respect to r and matches the streaming boundary layer solution.

Figure 7 displays isolines of the axial streaming velocity colored by its value and streamlines of the streaming flow obtained when the source term considered is $\frac{1}{r}\frac{\partial}{\partial r}(r\overline{v'_r v'_z})$. This source term is named the radial source term. The radial source term induces a streaming field of the same order of magnitude as the streaming field generated with the axial source term (see color code in Figures 5 and 7). Figure 8 shows the radial variation of the axial streaming velocity generated with the radial source term at different axial positions. The variation is parabolic in the core (as confirmed by a polynomial fit) and of the same order of magnitude as for the streaming generated with the axial source term. However the sign of the axial streaming velocity does not change inside the boundary layer therefore no streaming cell is generated in the boundary layer (compare Fig.6 and Fig. 8)). In order to understand this behaviour, we consider again an approximate equation in cylindrical coordinates, for a large resonator, outside the boundary layer:

$$\mu\frac{1}{r}\frac{\partial}{\partial r}(r\frac{\partial U_{2s}}{\partial r}) = \frac{\partial p_{2s}}{\partial z} + \rho_0\frac{1}{r}\frac{\partial}{\partial r}(r\overline{v'_r v'_z}) \quad . \tag{4}$$

The solution U_{2s} of Eq.4 is analytical. The correlation term $\overline{v'_r v'_z}$, like the radial acoustic velocity amplitude (see Fig. 3), varies linearly with the radial coordinate outside the boundary layer. The pressure term $\frac{\partial p_2}{\partial z}$ is constant with respect to r. The resulting analytical solution U_{2s} therefore has a parabolic profile in the radial direction.

The source term $\frac{\partial}{\partial z}\overline{v'_r v'_z}$ produces a streaming flow smaller in order of magnitude than U_{1s} and U_{2s}, rotating in the opposite direction. The streaming flow obtained considering the source term $\frac{1}{r}\frac{\partial}{\partial r}(r\overline{v'_r v'_r})$ is much smaller than all the other ones.

Finally, the axial source term is the only term responsible for creating the inner streaming cells.

3.2 Fast streaming flow

We carry on the same procedure for a higher intensity wave created with a forcing amplitude of $z_p = 10\ \mu m$. The streaming flow associated with such a wave can be placed in the second regime of streaming [8] with no extra cell generated. Figure 9 represents isolines of the axial streaming velocity colored by its value and streamlines of the streaming flow generated by the contribution of both the axial $\frac{\partial}{\partial z}(\overline{v'_z v'_z})$ and $\frac{\partial}{\partial z}(\overline{v'_r v'_z})$ source terms. Figure 10 displays isolines of the axial streaming velocity colored by its value

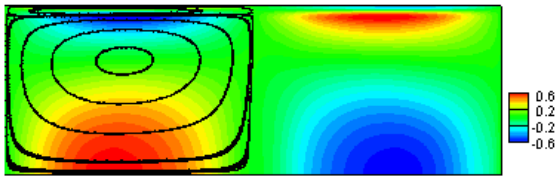

FIGURE 9 – Isolines of the axial streaming velocity colored by its value and streamlines of the streaming flow obtained with both the source terms $\frac{\partial}{\partial z}(\overline{v'_z v'_z})$ and $\frac{\partial}{\partial z}(\overline{v'_r v'_z})$, $z_p = 10\,\mu m$.

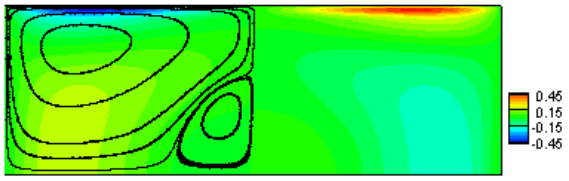

FIGURE 10 – Isolines of the axial streaming velocity colored by its value and streamlines of the streaming flow obtained in the case of the radial source term , $z_p = 10\,\mu m$.

and streamlines of the streaming flow generated by the radial source term alone.

In Figure 9 the streaming field is mainly due to the axial source term and no deformation can be observed on either inner or outer streaming flow patterns. On the contrary, the streaming flow due to the radial source term is strongly distorted : a new streaming cell appears on the axis of resonator, near the place of acoustic velocity anti-node (see Figure 10). When adding those two streaming fields in order to obtain the complete streaming flow field (neglecting the influence of the $\frac{1}{r}\frac{\partial}{\partial r}(r\overline{v'_r v'_r})$ source term), the order of magnitude of the axial streaming velocity in the core is smaller than the axial streaming velocity in the near-wall region. Moreover, the resulting streaming flow pattern does not exhibit a counter-rotating cell in the core.

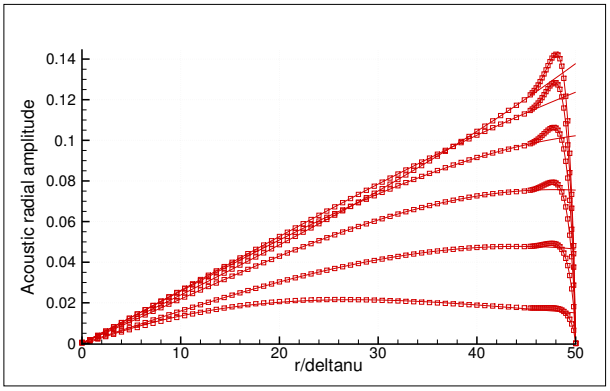

FIGURE 11 – Radial variation of the radial acoustic velocity obtained from the full DNS calculation at different axial locations, $z_p = 10\,\mu m$. Solid lines: polynomial fit in the core region.

Figure 11 shows the radial variation of the radial acoustic velocity v'_r at different axial positions obtained from the full DNS calculation. The profile is no longer linear in r, as it is in Regime 1, but is polynomial of 3rd order, as found by a polynomial fit in the core region. The corresponding streaming axial velocity profile in the radial direction is

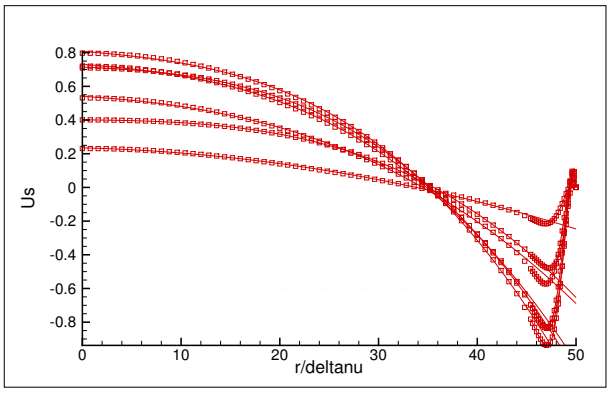

FIGURE 12 – Radial variation of the axial streaming velocity obtained with all the source terms at different axial locations, $z_p = 10\,\mu m$. Solid lines: polynomial fit in the core region.

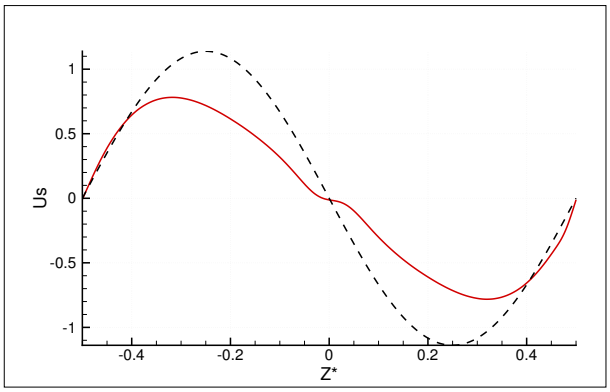

FIGURE 13 – Red line: axial variation of the axial streaming velocity at $r = 0$ obtained with all the source terms, $z_p = 10\,\mu m$. Dotted line: Rayleigh sinusoidal solution.

no longer parabolic in the center of the resonator but is polynomial of 3rd order as obtained by a polynomial fit in the core region (Figure 12).

Figure 13 shows the axial variation of the axial streaming velocity at $r = 0$ generated with all source terms. The obtained streaming profile is distorted compared to the sinusoidal Rayleigh solution. However no new cell emerges yet since the profile only changes sign at $z = 0$, i.e. at the place of transition between the two outer cells (Fig. 13). This is probably because the deformation due to the radial source term is not strong enough.

Finally, the radial source term appears to play a major role in the outer streaming pattern distortion in Regime 2. The radial acoustic velocity has a strong influence on this source term. In the next section, focus will be on the radial components and the possible interaction between acoustic and streaming flows.

3.3 Further discussion on fast streaming flow

In order to assess the interaction between acoustic and streaming flows, a DNS calculation is conducted where at the end of each period, the averaged flow over the preceding period is removed from the total velocity field. By doing so, we intend to artificially remove the influence of the streaming flow on the acoustic field. The resulting flow field gives an ”acoustic” field separated from the streaming flow. Figure 14 shows the radial variation of the resulting radial

acoustic velocity component for the case discussed in the previous section ($z_p = 10\ \mu m$). In the core region, the profile is linear just like it is for Regime 1 whereas the acoustic field extracted from the full DNS calculation has a radial component with a 3rd polynomial variation in the radial direction (Fig. 11).

This observation shows that streaming flow influences the acoustic field through the radial component.

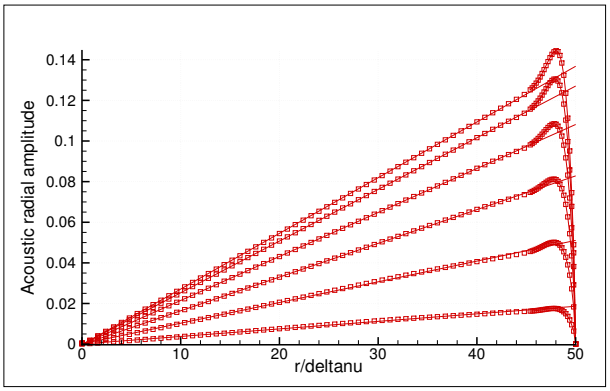

FIGURE 14 – Radial variation of the radial acoustic velocity at different axial locations when removing the influence of the streaming flow on the acoustic flow, $z_p = 10\ \mu m$. Solid lines: linear fit in the core region.

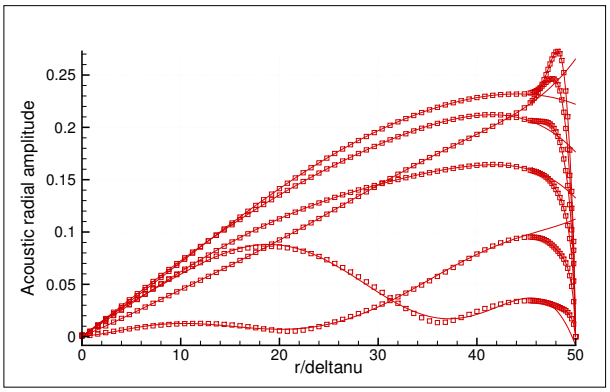

FIGURE 15 – Radial variation of the radial acoustic velocity obtained from the full DNS calculation at different axial locations, $z_p = 30\ \mu m$. Solid lines: polynomial fit in the core region.

The forcing amplitude is now increased to $z_p = 30\ \mu m$, which corresponds to a case in Regime 2 with an extra counter-rotating cell. Figure 15 displays the radial variation of the radial acoustic velocity obtained from the full DNS calculation at different axial locations. The profiles in the core are very distorted and correctly fitted by a polynomial of 6th order. Figure 16 shows the radial variation of the corresponding axial streaming velocity. The profiles in the core are correctly fitted by a polynomial of 5th order. On one of the profiles we can see negative values of the axial streaming velocity in the core, assessing the presence of the extra counter-rotating outer streaming cell.

Next we conduct again a DNS calculation where at the end of each period, the averaged flow over the preceding period is removed from the total velocity field. Figure 17 shows the radial variation of the corresponding radial acoustic velocity at different axial locations. The profiles are correctly fitted by a linear fit. Figure 18 shows the radial

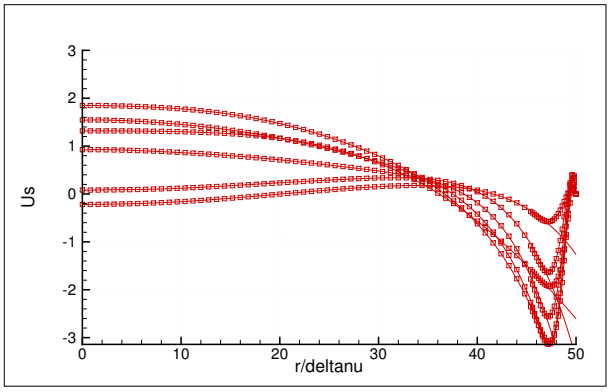

FIGURE 16 – Radial variation of the axial streaming velocity obtained from the full DNS calculation at different axial locations, $z_p = 30\ \mu m$. Solid lines: polynomial fit in the core region.

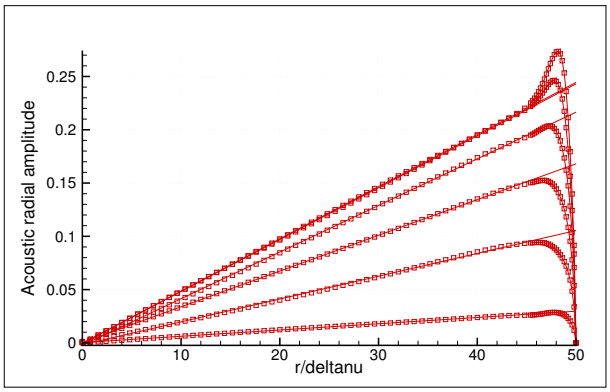

FIGURE 17 – Radial variation of the radial acoustic velocity at different axial locations when removing the influence of the streaming flow on the acoustic flow, $z_p = 30\ \mu m$. Solid lines: linear fit in the core region.

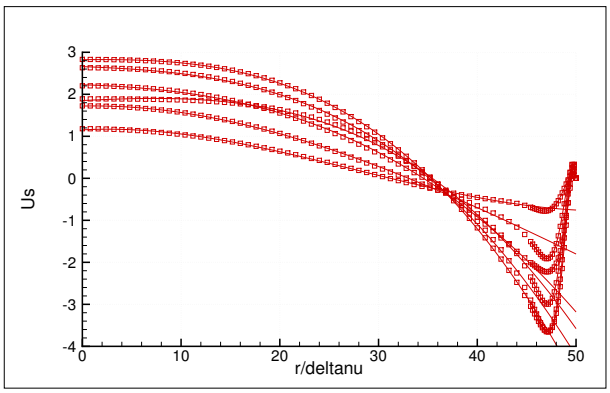

FIGURE 18 – Radial variation of the axial streaming velocity induced by the acoustic flow shown in Fig.17, $z_p = 30\ \mu m$. Solid lines: polynomial fit in the core region.

variation of the axial streaming velocity induced by the acoustic flow shown in Figure 17 calculated using the AMS code. The profiles are parabolic as shown by a polynomial fit and no extra cell is observed since the velocities are all positive in the core. The associated streaming pattern has a similar structure as a Regime 1 streaming flow pattern although created by a high intensity acoustic wave. This shows the major role played by the coupling between the streaming flow and the acoustic field. This coupling works as a two-way interaction through the radial components.

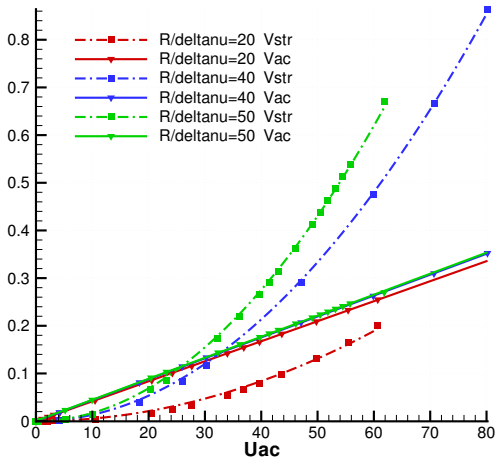

FIGURE 19 – Maximum radial streaming velocity (dotted lines) and radial acoustic velocity (solid lines) versus U_{ac}.

Let us now explore the relative amplitude of the radial acoustic and streaming velocity components. Figure 19 shows the maximum absolute value of radial streaming velocity (dotted lines) and radial acoustic velocity (solid lines) as functions of the axial acoustic velocity U_{ac} for several values of $R/\delta_\nu = 20, 40$ and 50. One can observe that the radial acoustic velocity dependence on U_{ac} is linear and is independent of R/δ_ν. The radial streaming velocity dependence is quadratic in U_{ac}. The amplitude of the radial streaming velocity increases with R/δ_ν. After the intersection of the two sets of curves the radial streaming velocity becomes significantly greater than the radial acoustic velocity for high values of R/δ_ν. On the other hand for the value $R/\delta_\nu = 20$, the radial streaming velocity is always smaller than the radial acoustic velocity for U_{ac} in the range [0 – 60] m/s. This is consistent with the transition from the first to the second regime of streaming as described in [8].

4 Conclusion

The influence of the radial component of the acoustic velocity on the streaming flow, as the streaming flow evolves from the first regime to the second regime was studied numerically. It was shown that the radial source term is responsible for the change of streaming behaviour. The radial acoustic velocity has a strong influence on this source term. Both the acoustic velocity and the radial source term were shown to be strongly modified in the second regime. The analysis of the variation of the radial acoustic and streaming velocities with respect to the acoustic amplitude U_{ac} shows that the radial streaming velocity component becomes greater than the radial acoustic velocity component in the second regime. The memory of the streaming flow influence on the acoustic field was artificially removed showing that the associated streaming pattern has a similar structure as a Regime 1 streaming flow pattern although created by a high intensity acoustic wave. This demonstrates that in Regime 2, the streaming flow distortion is mainly due to non linear interaction between acoustic and streaming flows through their radial components.

References

[1] L. Rayleigh, On the Circulation of Air Observed in Kundt's Tubes, and on Some Allied Acoustical Problems, *Philos. Trans. R. Soc.* **175**, 1-21 (1884)

[2] H. Bailliet, V. Gusev, R. Raspet, R. A. Hiller, Acoustic streaming in closed thermoacoustic devices, *J. Acoust. Soc. Am.* **114**, 3092-3101 (2001).

[3] M. F. Hamilton, Y. A. Ilinskii and E. . Zabolotskaya, Thermal effects on acoustic streaming in standing waves, *J. Acoust. Soc. Am.* **110**, 1808-1821 (2003).

[4] M.W. Thompson, A.A. Atchley, M.J. Maccarone, Influences ofa temperature gradient and fluid inertia on acoustic streaming in a standing wave, J. Acoust. Soc. Am. 117(4) (2004) 1839-1849.

[5] S. Moreau, H. Bailliet, J.-C. Valière, Measurements of inner and outer streaming vortices in a standing waveguide using laser doppler velocimetry, J. Acoust. Soc. Am. 123(2) (2008) 640-647.

[6] V. Daru, D. Baltean-Carlès, C. Weisman, P. Debesse and G. Gandikota, Two-dimensional numerical simulations of nonlinear acoustic streaming in standing waves, *Wave Motion* **50**, 955-963 (2013).

[7] V. Daru, D. Baltean-Carlès, C. Weisman, Inertial effects on non linear acoustic streaming, *AIP Conf. Proc.* **1685**, 030003 (2015).

[8] V. Daru, H. Bailliet, D. Baltean-Carlès, I. Reyt, C. Weisman, Transitoire et changement de régime des écoulements redressés de Rayleigh à forts niveaux : Études numérique et expérimentale, *CFA Proc.* (2016).

[9] L. Menguy, J. Gilbert, Nonlinear effect of the inertia of the fluid on acoustic streaming in cylindrical guides, *J. Acoust. Soc. Am.* **105**, 958-958 (1999).

[10] I. Reyt, V. Daru, H. Bailliet, S. Moreau, J. C. Valière, D. Baltean-Carlès and C. Weisman, Fast acoustic streaming in standing waves: Generation of an additional outer streaming cell, *J. Acoust. Soc. Am.* **134**(3), 1791-1801 (2013).